

## CLIMATOLOGY

## Greenland Ice Sheet surface melt amplified by snowline migration and bare ice exposure

J. C. Ryan<sup>1,2,\*</sup>, L. C. Smith<sup>1,2,3,\*</sup>, D. van As<sup>4</sup>, S. W. Cooley<sup>1,3</sup>, M. G. Cooper<sup>2</sup>, L. H Pitcher<sup>2</sup>, A. Hubbard<sup>5,6</sup>

Greenland Ice Sheet mass loss has recently increased because of enhanced surface melt and runoff. Since melt is critically modulated by surface albedo, understanding the processes and feedbacks that alter albedo is a prerequisite for accurately forecasting mass loss. Using satellite imagery, we demonstrate the importance of Greenland's seasonally fluctuating snowline, which reduces ice sheet albedo and enhances melt by exposing dark bare ice. From 2001 to 2017, this process drove 53% of net shortwave radiation variability in the ablation zone and amplified ice sheet melt five times more than hydrological and biological processes that darken bare ice itself. In a warmer climate, snowline fluctuations will exert an even greater control on melt due to flatter ice sheet topography at higher elevations. Current climate models, however, inaccurately predict snowline elevations during high melt years, portending an unforeseen uncertainty in forecasts of Greenland's runoff contribution to global sea level rise.

## INTRODUCTION

The Greenland Ice Sheet now contributes over 25% of observed global sea level rise, making it the largest single cryospheric contributor (1). Its enhanced mass loss over the 21st century (2, 3) is primarily attributed to increased surface meltwater runoff (4–6), of which ~93% derives from the relatively small ablation zone (~22% of the ice sheet area) along the ice sheet margin (7). As the winter snowpack melts during the summer, bare glacial ice is exposed in the ablation zone. Since bare ice is both darker and less porous than snow, it absorbs more than twice as much solar radiation and retains less meltwater. Bare ice therefore produces a large proportion (~78%) of Greenland's total runoff into the ocean (8), although it is only exposed across a small area of the ice sheet during the summer. Accurately capturing the reduced albedo and full extent of bare ice in climate models is therefore critical for determining Greenland's current and future runoff contributions to sea level rise (9).

Representing bare ice albedo and extent in climate models is challenging since both impart nonlinear positive feedbacks between net shortwave radiation and surface melt over seasonal time scales (7, 9–11). A seasonal increase in downward shortwave radiation reduces bare ice albedo through melt processes that darken the ice surface, notably, exposure of dust layers, pooling of surface meltwater, increased interstitial water content, and liquid meltwater-induced growth of pigmented ice algal assemblages that inhabit the bare ice surface (12–17). Despite operating over a relatively small area of the ice sheet, it is argued that these bare ice processes have contributed substantially to an observed reduction in albedo and associated increase in melt across Greenland's ablation zone from 2000 to 2011 (9, 14, 15). We collectively term this category of physical and biological melt-albedo processes that darken bare ice the “bare ice–albedo feedback”.

A seasonal increase in downward shortwave radiation also increases the extent of bare ice through the annual migration of the summer snowline. As sufficient energy is received at the surface to completely melt the accumulated winter snowpack, darker bare glacial ice is exposed, further enhancing the absorption of shortwave radiation by the ice sheet. We term this melt-albedo feedback the “snowline-albedo feedback.” While the importance of this process has long been recognized in alpine glacier settings (18–20), snowlines have received surprisingly little focus in Greenland beyond the pioneering facies work in the 1960s and 1990s (21–23). The importance of the snowline-albedo feedback for amplifying melt, and its efficacy relative to the bare ice–albedo feedback, has therefore yet to be evaluated.

Here, we assess the importance of the snowline-albedo feedback and its influence on Greenland Ice Sheet meltwater production using a new remotely sensed bare ice presence product (see Materials and Methods). We derive this product from daily Moderate Resolution Imaging Spectroradiometer (MODIS) satellite imagery acquired by NASA's Terra satellite and validated using Landsat 5, 7, and 8 satellite imagery and in situ field observations. We use our product to map snowline variability across Greenland from 2001 to 2017 and to evaluate its impact on the total net shortwave radiation relative to processes that darken bare ice and firn/snow. We then combine our snowline dataset with ice sheet surface topography to investigate how the strength of the snowline-albedo feedback changes as snowlines rise to higher elevations under a warmer climate. Last, owing to their heavy use for predicting future Greenland Ice Sheet melting and runoff contribution to global sea level rise, we assess whether regional climate models (RCMs) accurately determine snowline elevations.

## RESULTS

During the 2001–2017 study period, Greenland Ice Sheet snowline elevations exhibited substantial interannual variation (Fig. 1). Averaged across the ice sheet, end-of-summer (i.e., maximum) pan-Greenland snowline attained a maximum elevation of 1650 m in 2012 and a minimum of 1330 m in 2009, with a mean 2001–2017 elevation of  $1450 \pm 90$  m (mean  $\pm$  SD) (see Materials and Methods for the description of the snowline metric; Fig. 2). The pan-Greenland snowline elevation did not rise linearly over the entire 2001–2017 study period but rose significantly ( $R^2 = 0.50$ ;  $P < 0.01$ ) at an average

Copyright © 2019  
The Authors, some  
rights reserved;  
exclusive licensee  
American Association  
for the Advancement  
of Science. No claim to  
original U.S. Government  
Works. Distributed  
under a Creative  
Commons Attribution  
NonCommercial  
License 4.0 (CC BY-NC).

<sup>1</sup>Institute at Brown for Environment and Society, Brown University, Providence, RI, USA. <sup>2</sup>Department of Geography, University of California, Los Angeles, Los Angeles, CA, USA. <sup>3</sup>Department of Earth, Environmental and Planetary Sciences, Brown University, Providence, RI, USA. <sup>4</sup>Geological Survey of Denmark and Greenland, Copenhagen, Denmark. <sup>5</sup>Centre for Glaciology, Department of Geography and Earth Sciences, Aberystwyth University, Aberystwyth, UK. <sup>6</sup>Centre for Arctic Gas Hydrate, Environment and Climate, Department of Geology, University of Tromsø, Tromsø 9037, Norway.

\*Corresponding author. Email: jonathan\_ryan@brown.edu (J.C.R.); lsmith@geog.ucla.edu (L.C.S.)

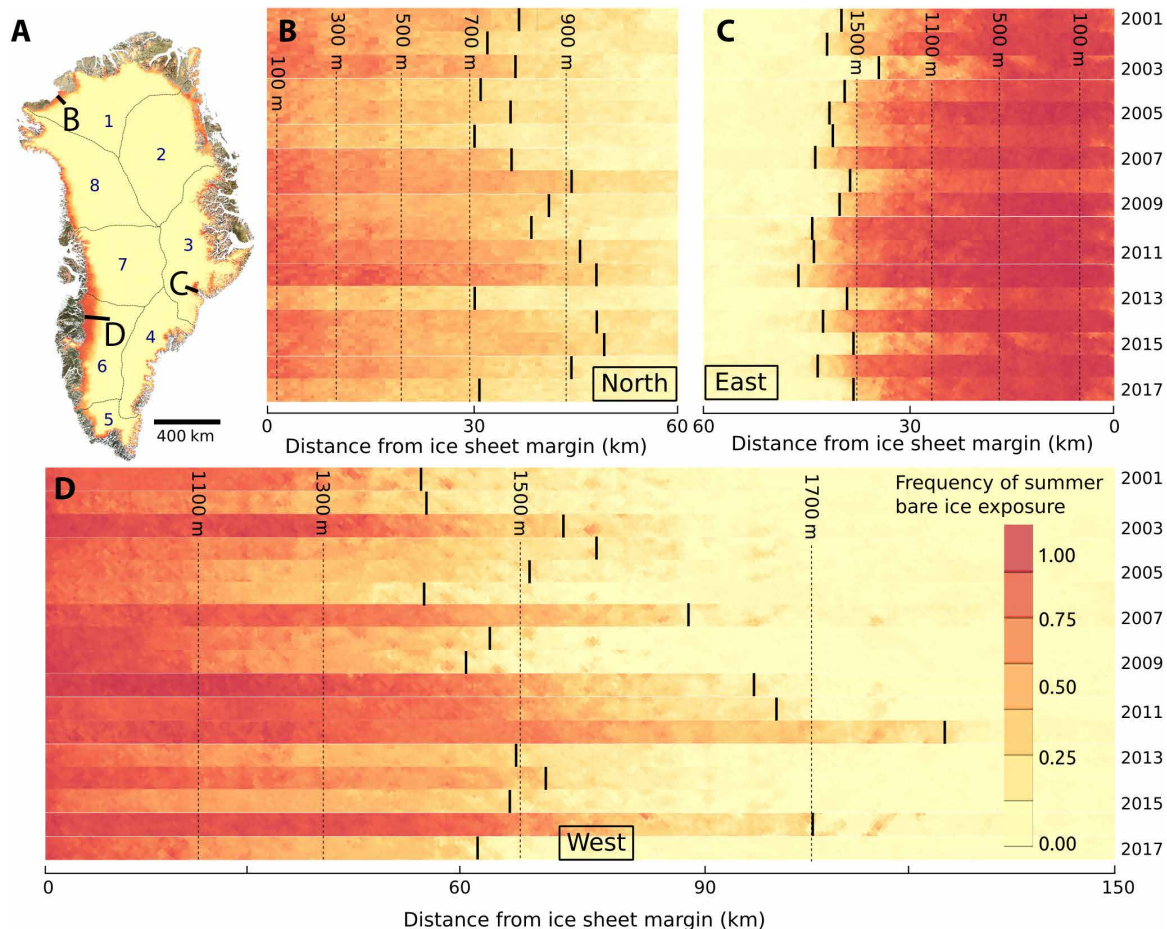


**Fig. 1. Interannual variations in frequency of summer bare ice exposure around the Greenland Ice Sheet over the study period (2001–2017).** A value of 1 indicates that bare ice was observed in every non–cloud contaminated summer June, July, and August (JJA) MODIS observation. Satellite-derived bare ice exposure maps were used to delineate the end-of-summer (maximum) snowline elevation (represented by vertical black lines) for each year. (A) Pan-Greenland bare ice exposure averaged over the 2001–2017 study period. Black lines denote the IMBIE sectors used for regional analysis. Numbered labels are as follows: 1, North; 2, Northeast; 3, East; 4, Southeast; 5, South; 6, Southwest; 7, West; and 8, Northwest Greenland. (B) Frequency of bare ice exposure and snowline elevation at Humboldt Glacier, North Greenland. (C) Frequency of bare ice exposure and snowline elevation at Kangerlussuaq Glacier, East Greenland. (D) Frequency of bare ice exposure and snowline elevation across the K-transect of automated weather stations (AWSs) in Southwest Greenland. The location of each transect is displayed in (A). Note that the x-axis scale is the same for (B) to (D).

rate of 17 m per year ( $a^{-1}$ ) from 2001 to 2012 (Fig. 2A). Spatially, end-of-season snowline elevations exhibited substantial regional variation, generally rising with decreasing latitude and ranging from  $980 \pm 67$  m (mean  $\pm$  SD) in North Greenland to  $1520 \pm 113$  m in Southwest Greenland (see tables S1 and S2). In general, end-of-summer snowline elevations displayed greatest variability in Southwest Greenland (varying by  $\pm 385$  m over the 2001–2017 study period; Fig. 1D) and least variability in East Greenland (varying by  $\pm 132$  m over the 2001–2017 study period; Fig. 1C).

Because the position of the seasonal snowline is the primary determinant of bare ice exposure, bare ice extent closely tracks interannual variations in snowline elevation (Fig. 2). End-of-summer pan-Greenland bare ice extent averaged  $221,890 \pm 30,120$  km<sup>2</sup> ( $12 \pm 2\%$  of the total ice sheet area; mean  $\pm$  SD) over the 2001–2017 study period. The maximum mapped bare ice extent ( $300,050$  km<sup>2</sup>) occurred in summer 2012, a record-setting melt year when bare ice was exposed across 16% of the ice sheet. In contrast, the smallest mapped extent of bare ice ( $184,660$  km<sup>2</sup>) occurred in 2006, when bare ice was exposed across just 10% of the ice sheet (Fig. 2), nearly 40% percent less area than

that in 2012. Like snowline elevation, bare ice extent did not exhibit any discernible temporal trend over the 2001–2017 study period ( $P > 0.10$ ) but increased significantly by  $6950$  km<sup>2</sup>  $a^{-1}$  between 2001 and 2012 ( $R^2 = 0.55$ ;  $P < 0.01$ ) an average increase of 4.1% per year ( $a^{-1}$ ). We provide regional quantifications of both snowline elevation and bare ice extent, together with an uncertainty analysis, in tables S1 and S2.

We demonstrate the importance of snowline migration on overall ice sheet melt production by quantifying how fluctuations in bare ice extent affect net shortwave radiation, the dominant contributor of Greenland Ice Sheet melt energy (24, 25). To do this, we combine our daily bare ice presence product with daily albedo data from MODIS (MOD10A1) and daily downward shortwave radiation fields from Modèle Atmosphérique Régional (MAR) 3.9 (26), to partition the total shortwave radiation absorbed by bare ice versus firn/snow in the ablation zone [i.e., where net surface mass balance (SMB) is  $<0$ ] (see Materials and Methods). Net shortwave radiation is then partitioned again by fixing the albedo of bare ice to the mean bare ice albedo observed on June 1 during the 2001–2017 study

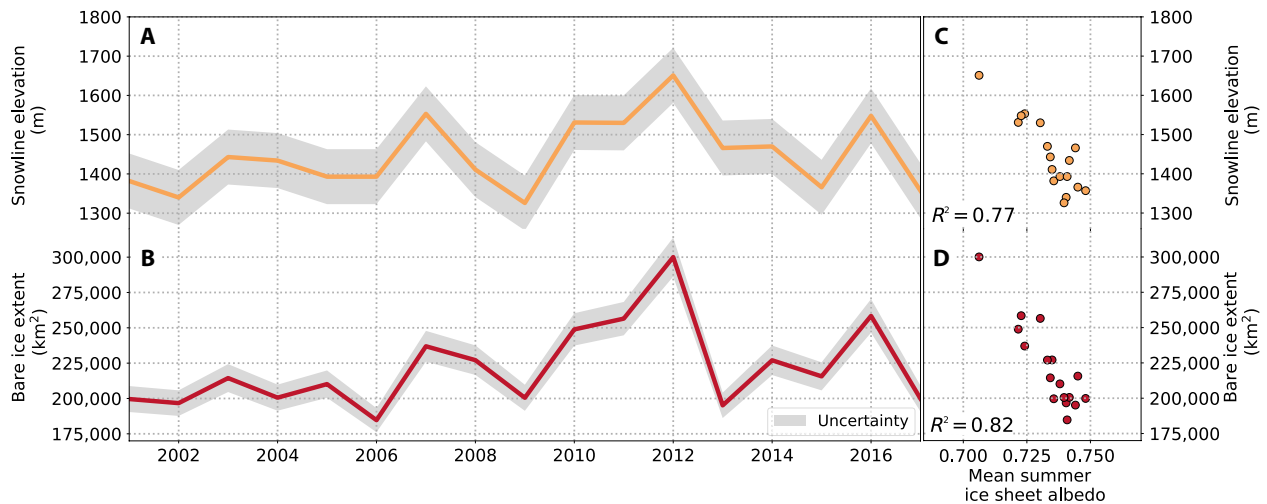


**Fig. 2. Interannual variations in observed end-of-summer snowline elevation and bare ice extent across the Greenland Ice Sheet from 2001 to 2017.** (A) End-of-season (or maximum) snowline elevation; (B) maximum bare ice extent. Gray shaded areas represent the uncertainty of both metrics (see Materials and Methods). Neither metric exhibits a statistically significant linear trend over the entire study period ( $P > 0.10$ ), partly owing to low snowline elevation and bare ice extent in 2013 and 2017. However, snowline elevation and bare ice extent increased significantly ( $P < 0.01$ ) between 2001 and 2012, a period of declining albedo on the ice sheet often attributed to hydrological and/or biological processes that darken the ice sheet surface. Relationship between (C) snowline elevation and (D) bare ice extent with mean summer pan–Greenland Ice Sheet albedo. Both metrics are significantly correlated, indicating that the area of bare ice exposure and total ice sheet albedo are closely coupled.

period. The residual difference between the shortwave energy absorbed by bare ice with fixed albedo and bare ice with observed albedo allows us to evaluate the efficacy of increasing bare ice extent versus decreasing bare ice albedo on melt.

We find that net shortwave radiation in the ablation zone is primarily controlled by fluctuations in bare ice extent during the 2001–2017 study period (Fig. 3A). Net shortwave radiation attributed solely to variations in the extent of bare ice (and corresponding extent of firn/snow) had an SD of  $\pm 9$  exajoules (EJ;  $10^{18}$  J) during our study period, equivalent to 53% of the total net shortwave radiation variability in the ablation zone ( $\pm 17$  EJ). This is exemplified by years 2010 and 2012, when an additional 12 EJ (7%) and 18 EJ (11%) of shortwave energy were absorbed in the ablation zone relative to the 2001–2017 mean solely because snowlines rose earlier in the season and to higher elevations (Fig. 3A). These energy quantities are equivalent to +36 and +54 Gt of additional melt, when converted to mass using the latent heat of fusion for ice ( $334$  kJ  $\text{kg}^{-1}$ ). Since shortwave radiation is the dominant contributor of ice sheet melt energy, it follows that interannual fluctuations in bare ice extent, driven by snowline migration, were an important control on ice sheet meltwater production during the 2001–2017 study period.

Other processes that reduce the albedo of bare ice and firn/snow also influence interannual variations in net shortwave radiation in the ablation zone. Excluding the effects of snowline fluctuations, shortwave radiation absorption attributed to temporal variability in bare ice albedo and firn/snow albedo had an SD of  $\pm 5$  and  $\pm 3$  EJ during the study period, accounting for 29 and 18% of the total net shortwave radiation variability in the ablation zone, respectively (Fig. 3A). In 2010 and 2012, the reduction in bare ice albedo increased net shortwave radiation absorbed in the ablation zone by 4 and 5%, respectively, relative to the 2001–2017 mean. However, while processes that darken bare ice [e.g., exposure of dust (13), presence of surface and interstitial water (12), and algal growth (14–17)] and snow [e.g., impurities and snow grain size (7, 11)]

are important amplifiers of melt, our analysis suggests that they are secondary in comparison to processes that expose bare ice (i.e., snowline migration).

Seasonally (i.e., from June 1 to August 31), we find that increasing bare ice extent, rather than decreasing bare ice albedo, is the primary driver of shortwave radiation absorption in the ablation zone when averaged over the entire 17-year study period (Fig. 3B). From 2001 to 2017, a mean 84% (77 EJ) of the total shortwave radiation absorbed by bare ice was due to its increasing extent. In contrast, the mean net shortwave radiation due to the seasonal decline in bare ice albedo (15 EJ) was just a fifth of the additional net shortwave radiation due to increases in bare ice extent (Fig. 3B). This may be explained, at least partly, by the magnitude of albedo reduction caused by bare ice darkening processes. The mean reduction of bare ice albedo over the summer (from June 1 to August 31) was 0.12 (i.e., from 0.57 to 0.45). In contrast, the difference between the albedo of firn/snow and bare ice is almost double (i.e., 0.22, from 0.79 to 0.57). The strongest melt-albedo feedback operating on the Greenland Ice Sheet is therefore caused by rising seasonal snowlines, rather than biological and/or hydrological processes that alter the bare ice albedo itself.

Because of differences in ice sheet hypsometry (i.e., the relationship between surface area and elevation) and climate, the strength of the snowline-albedo feedback varies regionally around the ice sheet (27, 28). To assess where the snowline-albedo feedback had greatest impact during the 2001–2017 study period, we subdivide our net shortwave radiation analysis into eight ice sheet sectors based on the Ice Sheet Mass Balance Inter-comparison Exercise (IMBIE) (Fig. 1A). We then evaluate the sensitivity of each sector to the snowline-albedo feedback by quantifying the relative impact of snowline fluctuations on bare ice extent and total net shortwave variability in the ablation zone [i.e., the SD of shortwave radiation absorbed by bare ice extent from 2001–2017 divided by the mean shortwave radiation absorbed by bare ice extent from 2001–2017,

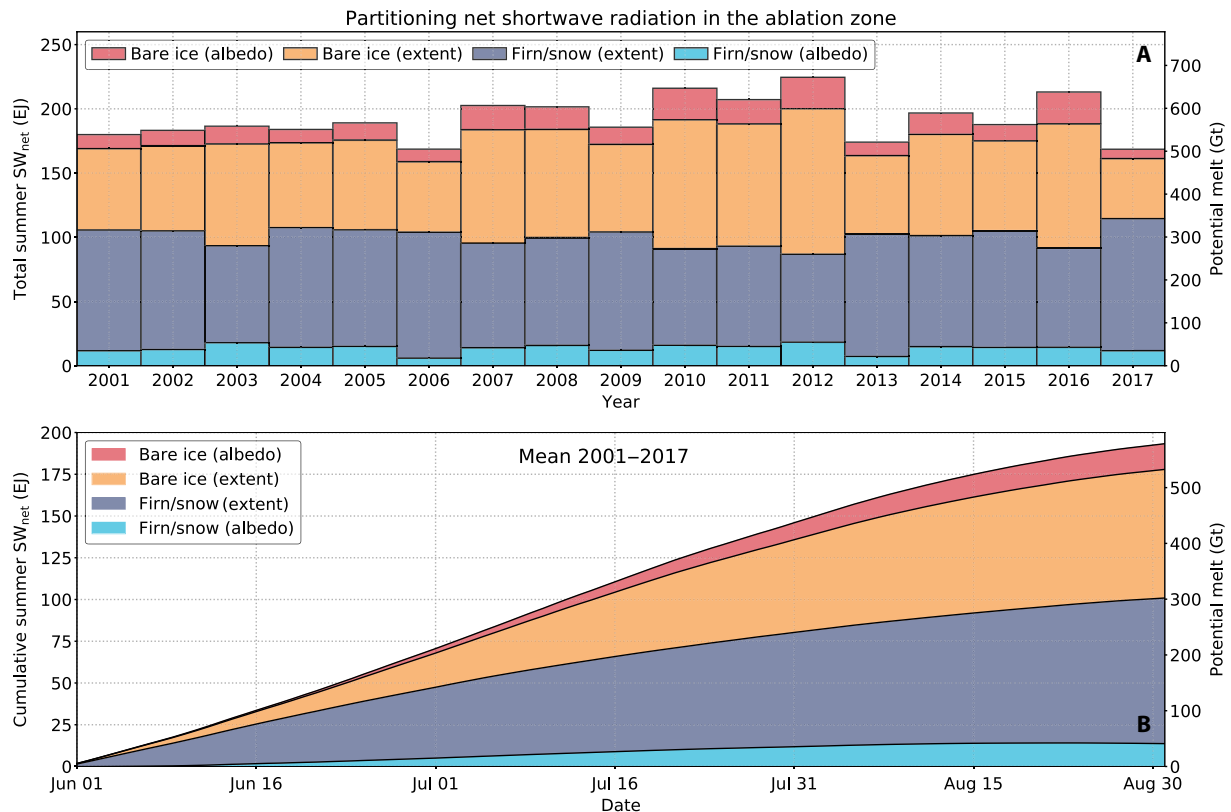


**Fig. 3. Partitioned net shortwave radiation absorbed by the Greenland Ice Sheet ablation zone over the 2001–2017 study period, in units of energy (exajoules) and mass (gigatons of potential melt).** (A) Interannual variations; (B) cumulative summer (JJA) average. In each figure, net shortwave ( $SW_{net}$ ) radiation is partitioned into radiation absorbed by firn/snow albedo (turquoise), firn/snow extent (blue), bare ice extent (orange), and bare ice albedo (red). Interannual fluctuations in bare ice extent (and corresponding fluctuations in firn/snow extent) drive most of the variation in net shortwave radiation, signifying that the processes that expose bare ice (e.g., snowline migration) are the strongest melt-albedo feedback operating on the ice sheet.

i.e., the coefficient of variation ( $C_v$ )). This allows assessment of which sectors of the ice sheet are most sensitive to the snowline-albedo feedback due to the current topographic hypsometry of the ice sheet surface.

We find that Southwest Greenland (IMBIE sector 6) was the most sensitive sector to the snowline-albedo feedback ( $C_v = 0.31$ ) during the 2001–2017 study period. Of the total shortwave radiation absorbed by bare ice, 42% was absorbed in this sector. This is because the gently sloping ice surface topography of Southwest Greenland, together with mild summer air temperatures and low snow accumulation (9), exposes large areas of bare ice every summer as the regional snowline rises to higher elevation (e.g., Fig. 1A). In this sector, small increases/decreases in melt cause large increases/decreases in snowline and associated bare ice exposure. This is exemplified by the difference between 2012 and 2013, when a reduction in bare ice extent reduced summer shortwave radiation absorption in the ablation zone by 7 EJ (potential melt, 21 Gt) equivalent to 54% of the total reduction in net shortwave radiation in the ablation zone in this sector [13 EJ; (potential melt, 39 Gt)]. The snowline-albedo feedback is thus strongest in Southwest Greenland.

The coefficient of variation indicates that the snowline-albedo feedback also drives large fluctuations in shortwave energy absorbed in North ( $C_v = 0.28$ ), Northeast ( $C_v = 0.25$ ), South ( $C_v = 0.27$ ), and Northwest Greenland ( $C_v = 0.26$ ) (Fig. 1A). Although less bare ice is exposed in these sectors (e.g., Fig. 1, B and D), they either have gently

sloping ice surface topography (e.g., North and Northeast Greenland) or experience large interannual climatic variations (e.g., variable winter snowfall), which induce large interannual variations in summer bare ice exposure. In contrast, the coefficient of variation in East ( $C_v = 0.19$ ) and Southeast ( $C_v = 0.23$ ) Greenland is smaller, indicating that the topography and climate of these sectors act to suppress snowline variability and associated fluctuations in net shortwave radiation. An example of this is East Greenland where steep ice surface topography constrains interannual variations in bare ice exposure (Fig. 1D).

Summer air temperatures over the Greenland Ice Sheet are projected to increase up to 4.1°C by the end of the 21st century (29). Snowlines will likely rise to higher elevations than the range that we observe during our 2001–2017 study period (Fig. 4, gray shaded area). This will, depending on the ice sheet hypsometry, cause the snowline-albedo feedback to intensify. To evaluate the hypsometric sensitivity of the snowline-albedo feedback, we calculate the area of new bare ice exposure that would be introduced by raising the snowline up to 500 m above the corresponding mean 2001–2017 elevations [Fig. 4 (red shaded area) and fig. S1]. This metric (in units of square kilometer of bare ice exposed per meter of snowline elevation change) enables the assessment of the potential amplification of the snowline-albedo feedback under a future warmer climate.

Our results demonstrate that the area of bare ice exposure per meter of snowline elevation rise increases exponentially in all sectors

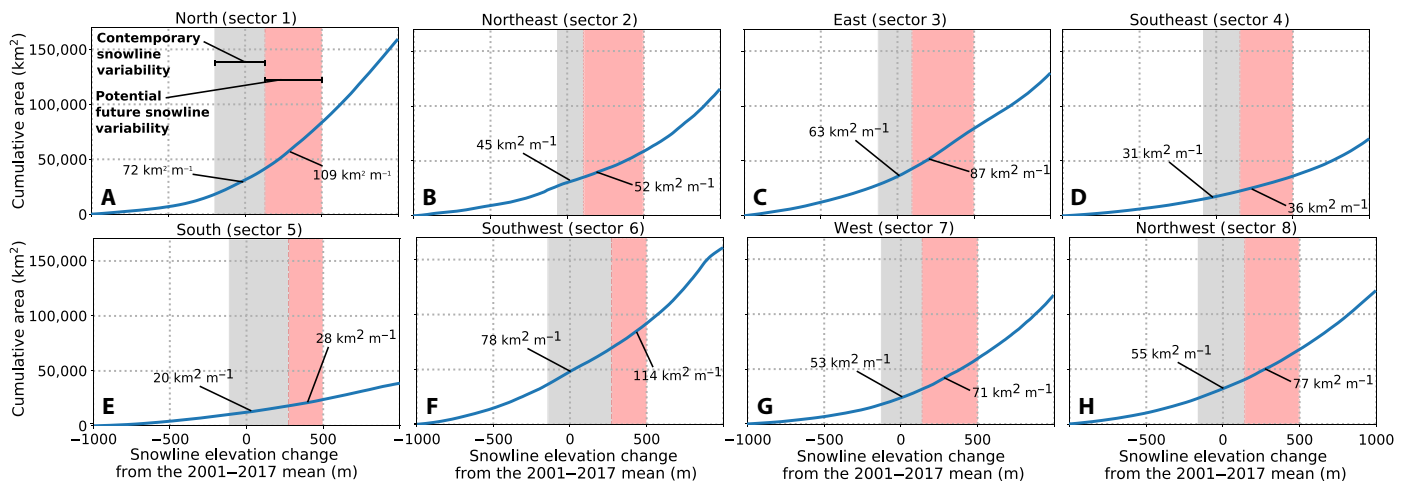


**Fig. 4. Hypsometric surface elevation-area relationships for all eight IMBIE Greenland sectors.** Gray shaded areas indicate the observed range of snowlines and bare ice areas that we mapped using MODIS satellite imagery from 2001 to 2017. Red shaded areas indicate the estimated range of snowlines and bare ice areas that would occur if end-of-summer snowlines rise 500 m higher than the 2001–2017 mean. Labels summarize rate-of-change of bare ice exposure in units of area per meter increase in snowline ( $\text{km}^2 \text{m}^{-1}$ ). All hypsometric relationships are computed using the Greenland Ice Mapping Project (GIMP) digital elevation model (37) and assume static, present-day surface topography. The exponential relationships suggest that strength of the snowline-albedo feedback reported here will become stronger in the future as snowlines rise to higher, flatter areas of the ice sheet, owing to increasing areas of bare ice exposed per unit rise in snowline elevation.

because of a flatter ice sheet surface at higher elevations. This nonlinear increase of bare ice exposure signifies that the impact of Greenland's snowline-albedo feedback will become even stronger as snowlines rise, including areas other than Southwest Greenland. In North Greenland, for example, the strength of the snowline-albedo feedback increases by 51% relative to our 2001–2017 study period (Fig. 4A). In East, Southwest, West, and Northwest Greenland, it increases by between 30 and 40% relative to the present day (Fig. 4, C and F to H). In contrast, the snowline-albedo feedback does not intensify substantially in Northeast, Southeast, and South Greenland, where current elevation-area relationships remain relatively constant under a scenario of 500 m of snowline elevation rise (Fig. 4, B, D, and E).

## DISCUSSION

In principle, the current generation of physically based RCMs should capture the contemporary and future strength of the snowline-albedo feedback, since they couple sophisticated multilayer snow models with realistic ice sheet surface topography (6, 8, 26, 30, 31). However, we find that two RCMs commonly used for forecasting Greenland meltwater runoff [MAR3.9 (26) and Regional Atmospheric Climate Model (RACMO) 2.3p2 (30)] do not accurately capture maximum snowline elevations and bare ice extent (Fig. 5). In comparison to our remotely sensed bare ice presence metrics, we find that, on average, RACMO2.3p2 underestimates maximum bare ice extent by 6%, while MAR3.9 overestimates by 13% during the 2001–2017 study period (Fig. 5, A and B and fig. S2). Furthermore, we find that these discrepancies are significantly correlated with total summer runoff (Fig. 5, C and D). This suggests that MAR3.9 and RACMO2.3p2 do not sufficiently capture the role of the snowline-albedo feedback during extreme melt years (e.g., 2010, 2012, and 2016). Given that bare ice exposure is a primary control on meltwater production (Fig. 3) and that extreme melt events are projected to increase in the future (29), the failure of RCMs to accurately predict snowline elevation and bare ice extent during high melt years raises uncertainty in 21st-century forecasts of Greenland's future runoff contribu-

tions to global sea level rise (Fig. 6). Moreover, uncertainty in bare ice extent adds an additional challenge for modeling the spatio-temporal variability of bare ice albedo and its impact on future runoff (15, 17).

Our findings indicate that future projections of ice sheet runoff by the current generation of semi-empirical models (e.g., positive-degree day or temperature index) must also be treated with caution. These models, which are typically calibrated to RCM-modeled runoff, assume that the strength of melt-albedo feedbacks observed in the past remains constant into the future (32–34). However, since the snowline-albedo feedback is not accurately captured by RCMs and bare ice exposure increases nonlinearly as snowlines rise, this assumption appears unjustified. If semi-empirical models are to be used for forecasts of Greenland's future contribution to sea level rise, then they should therefore account for the increasing strength of melt-albedo feedbacks, such as that induced by snowline migration.

Our study quantifies, for the first time, the importance of Greenland's snowline for amplifying ice sheet melt. We find that snowlines exhibit substantial seasonal and interannual variation and are the dominant control on shortwave energy absorption and meltwater production in the ablation zone. While hydrological and biological processes that darken bare ice also influence shortwave energy absorption and runoff generation, they are secondary to the extent of bare ice exposure associated with snowline fluctuations. Unless offset by enhanced winter accumulation, snowlines will rise to higher elevations in a warmer climate and seasonally amplify melt even more than they presently do because of the hypsometry of the ice sheet. Since bare ice has much lower porosity than snow and firn, rising snowlines will reduce not only ice sheet albedo but also the capacity of the ice sheet to retain meltwater. Furthermore, since bare ice has substantially higher surface roughness than snow, the exposure of bare ice will also increase the rate of turbulent heat transfer from the atmosphere to the ice sheet surface. Improved representation of snowlines and bare ice exposure in climate models is therefore critical for accurately projecting future Greenland Ice Sheet runoff contributions to global sea level rise.

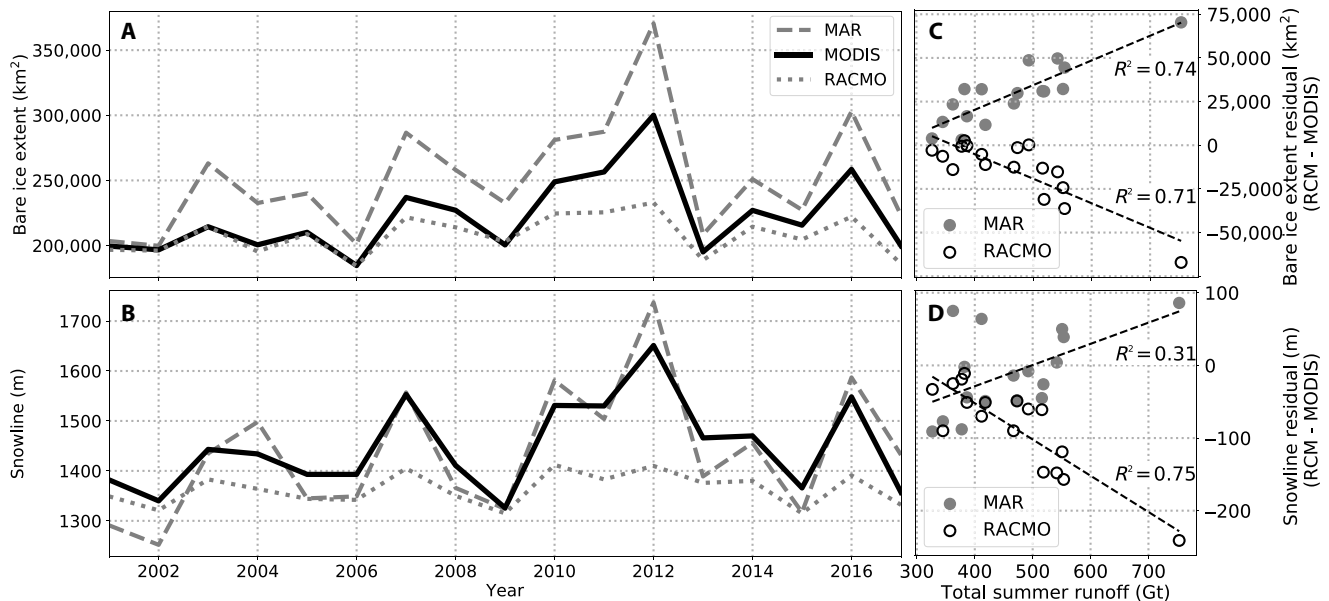


**Fig. 5. Comparison between observed (MODIS) and modeled (MAR3.9 and RACMO2.3p2) bare ice extent and snowline during the 2001–2017 study period.** Interannual variations in (A) maximum bare ice extent and (B) maximum snowline elevation. The residual between observed and modeled (C) bare ice extent and (D) snowline is greatest during years with higher runoff, because RACMO2.3p2 does not expose enough bare ice while MAR3.9 exposes too much. Note that the timing of bare ice exposure is also modeled inaccurately during high melt years (see fig. S2). These discrepancies introduce uncertainties in RCM forecasts of future Greenland runoff contributions to sea level rise.

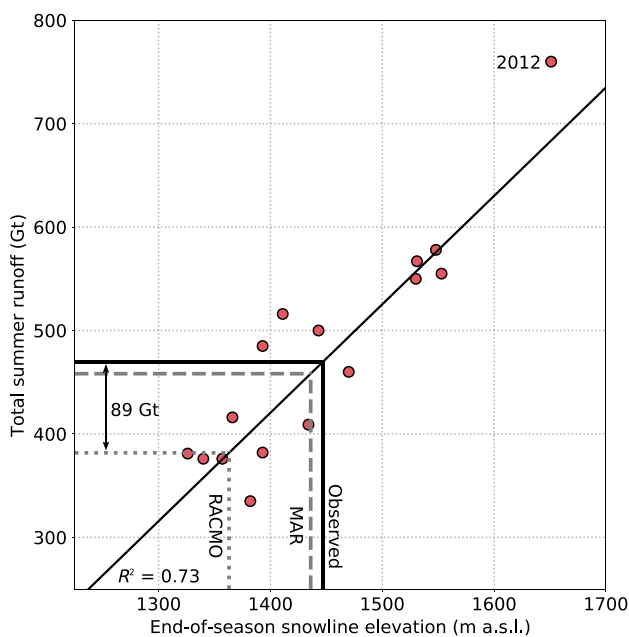


**Fig. 6. Relationship between end-of-season snowline elevation and total summer runoff during the 2001–2017 period ( $R^2 = 0.73$ ).** Note that both variables are modeled by MAR3.9. The labeled lines indicate the mean end-of-season snowline observed by this study (solid), modeled by RACMO2.3p2 (dotted), and modeled by MAR3.9 (dashed) over the 2001–2017 study period. The strong positive correlation between snowline and runoff indicates that accurate representation of snowlines in climate models is critical for accurate forecasts of Greenland Ice Sheet runoff.

**MATERIALS AND METHODS**

**Data**

MOD09GA daily land surface reflectance Collection 6 products for every summer (June 1 to August 31) between 2001 and 2017 were downloaded from NASA’s Land Processes Distributed Active Archive Center (LP DAAC) at the U.S. Geological Survey (USGS) Earth Resources Observation and Science (EROS) Center. The MOD09GA product provides atmospherically corrected surface reflectance from Terra’s MODIS for bands 1 to 7. The product was collected daily and delivered on a sinusoidal grid with a grid cell resolution of  $\sim 0.25 \text{ km}^2$ . MOD10A1 daily snow cover Collection 6 data were also downloaded from 2001 to 2017 from NASA’s National Snow and Ice Data Center Distributed Active Archive Center. MOD10A1 was collected daily and delivered on a sinusoidal grid with a grid cell resolution of  $\sim 0.25 \text{ km}^2$ . We noted that MOD10A1 Collection 6 accounts for Terra MODIS sensor degradation, which was uncorrected for in the previous collection (C5) (35, 36). The eight MOD09GA and MOD10A1 tiles that cover Greenland (h15v01, h15v02, h16v00, h16v01, h16v02, h17v00, h17v01, and h17v02) were mosaicked, re-projected to North Pole Stereographic (ESRI:102018), and resampled (nearest neighbor) to a pixel resolution of  $500 \times 500 \text{ m}$ . The mosaic was then clipped using the Greenland Ice Mapping Project (GIMP) ice mask (37). A cloud mask was produced by combining the pixels flagged as clouds in MOD10A1 with the MOD09GA cloud-state layer. Data from Aqua’s MODIS instrument were not used in this study because a failure in band 6 reduces cloud detection capability (7).

**Classification**

Discrimination between bare ice and firn/snow was achieved using random forests supervised classification (fig. S3) (38). We first produced a training dataset by manually classifying pixels as bare ice,

snow, or water in the MOD09GA and MOD10A1 composite images. Field in situ portable spectrometer measurements made between 2014 and 2016 indicate that the greatest differences in spectral reflectance between ice and snow occur in the visible wavelengths. The red (band 1: 620 to 670 nm), green (band 4: 545 to 565 nm), and blue (band 3: 459 to 479 nm) bands were therefore used for distinguishing between ice and snow during the manual digitization process (e.g., fig. S4). Where the surface type was unclear in the MODIS visible-band composites, higher-resolution (30 m) Landsat 5 Thematic Mapper (TM), Landsat 7 Enhanced Thematic Mapper-plus (ETM+), and Landsat 8 Operational Land Imager (OLI) orthorectified, top-of-atmosphere reflectance images (L1T) were used to guide manual classification.

A total of 5359 MODIS pixels spread across different sectors of the ice sheet were manually classified on the basis of their spectral attributes. Of these pixels, 3631, 1408, and 320 were identified as snow, bare ice, and water, respectively. The training dataset is available upon request from the authors. For testing purposes, a random subsample containing 20% of the pixels was removed from training dataset. The remaining bare ice, snow, and water samples were used to train the random forests classification, which was subsequently used to classify all summer MOD09GA and MOD10A1 mosaics between 2001 and 2017. Since snow and ice are best distinguished in the visible and near-infrared wavelengths, only non-cloud contaminated pixels in a MODIS composite containing MOD09GA bands 1 (620 to 670 nm), 2 (841 to 876 nm), 3 (459 to 479 nm), and 4 (545 to 565 nm) and the MOD10A1 albedo layer were considered for classification (figs. S3 and S4).

### Validation

Initial testing using the subsample of pixels removed before training revealed that the random forests classification has a classification accuracy of 99.3%. More rigorous evaluation of classification performance was judged by calculating errors of bare ice omission (i.e., bare ice incorrectly classified as snow) and commission (i.e., snow incorrectly classified as bare ice). We evaluated these errors by comparing classified MODIS pixels with coincidentally acquired (i.e., same day) Landsat 5 TM, 7 ETM+, 8 OLI pixels, which were treated as “ground truth” (i.e., zero error) (fig. S3). Bare ice and snow pixels were manually digitized in the higher-resolution satellite imagery between 2001 and 2017 using Google Earth Engine. Manual digitization was undertaken using multiband Landsat L1T composites containing visible and near-infrared bands to improve discrimination between bare ice and snow. To ensure fair consideration of uncertainties, pixels were sampled in close proximity to the snowline. In total, a sample of 133,588 Landsat pixels were obtained. Of these pixels, 61,108 were dedicated to the estimation of omission (i.e., Landsat pixels identified as bare ice), and 72,480 pixels were dedicated to commission (i.e., Landsat pixels identified as snow). When compared to the MODIS classification, we found that errors of bare ice omission were 4.6% and errors of bare ice commission were 0.3%. The higher errors of omission mean that we likely underestimate rather than overestimate bare ice presence, making our bare ice extent and snowline metrics (described in the next paragraphs) conservative (Fig. 2). Overall, we find that bare ice is classified with an average accuracy of 97.8% based on comparison with Landsat imagery.

### Bare ice presence index

The daily classified bare ice maps derived from MODIS were used to calculate a summer June, July, and August (JJA) bare ice presence

index (or exposure frequency) (fig. S5). The bare ice presence index varies between 0 and 1 in any given summer and is defined as the number of times a pixel is classified as bare ice divided by the total number of valid observations of that pixel (i.e., when not cloud-obscured) between June 1 and August 31. The mean number of valid pixel observations for the whole ice sheet ranged between 45 and 61 days (50 to 68%) and averaged 56 days (62%) between 2001 and 2017. We find that there is some variability between the number of valid observations in June, July, and August (fig. S6). However, the variability is small ( $SD = \pm 1.3$  days) and cannot explain the observed fluctuations of bare ice presence between 2001 and 2017. Seasonal variability in the number of valid observations therefore does not appear to have biased our results (fig. S6).

Validation of the bare ice presence index was achieved with comparison to in situ albedo measurements derived from 21 PROMICE/GAP automated weather station (AWS) measurements around the ice sheet (39). AWS albedo is measured by Kipp & Zonen CNR1 or CNR4 net radiometers, which measure downward and upward short-wave radiation fluxes with a specified uncertainty of less than 5% (40). Downward shortwave radiation was corrected for tilt and was only calculated when solar zenith angles were larger than 70°. Daily albedo was calculated by integrating the hourly averaged albedo data over a 24-hour period. Bare ice was defined as daily albedo  $< 0.55$ , and summer bare ice presence index was calculated in the same way as the MODIS bare ice maps. This threshold is based on in situ portable spectrometer and unmanned aerial vehicle (UAV) albedo measurements, which indicate that bare ice is rarely brighter than 0.55. We find that our MODIS bare ice presence product is in close agreement with that measured by the AWS with an  $R^2$  equal to 0.82 (fig. S7).

### Metrics

The annual maximum elevation of the snowline and extent of bare ice were derived from the summer bare ice presence index maps (fig. S5). The annual maximum extent of bare ice is defined as the number of pixels having a bare ice presence index of  $> 0.1$ . This value was chosen to protect against potentially misclassified pixels and makes the maximum bare ice extent metric conservative. Interannual variations of end-of-summer bare ice extent for the entire ice sheet are presented in Fig. 2. End-of-summer bare ice extent is also provided for each of the eight IMBIE sectors in tables S1 and S2.

The annual maximum snowline elevation, corresponding to the end-of-summer snowline in alpine glaciology literature, is defined as the 90th percentile of bare ice pixel elevations (i.e., those with a bare ice presence of  $> 0.1$ ) (41) (fig. S5). The elevation of each pixel was derived from the GIMP digital elevation model (37). The 90th percentile was chosen to protect against potentially misclassified pixels and makes the end-of-summer snowline metric conservative. We note that the end-of-summer snowline metric is a useful relative summary metric for assessing and conceptualizing interannual changes of bare ice exposure but has limited usefulness as an absolute metric due to strong latitudinal gradients of snowline elevation across the ice sheet (e.g., fig. S5). To account for latitudinal snowline variations, we provided end-of-season snowline elevation for each IMBIE sector in tables S1 and S2.

The uncertainties of both metrics were evaluated by considering the errors of commission (0.3%) and omission (4.6%) in the bare ice classification. By incorporating these uncertainties into our metrics, we find that maximum summer bare ice extent may be overestimated by 790 km<sup>2</sup> and underestimated by up to 12,103 km<sup>2</sup>. Likewise, the

end-of-season snowline may be overestimated by 5 m and underestimated by up to 70 m. We consider these uncertainties when the remotely sensed metrics were compared with similar metrics derived from RCMs.

### Albedo and downward shortwave radiation

Daily ice sheet albedo from 2001 to 2017 was obtained from the albedo layer (300 to 3000 nm) in the MOD10A1 C6 product. MOD10A1 is a “blue-sky” albedo product, meaning that it is a linear combination of directional-hemispherical reflectance (“black-sky albedo”) and bi-hemispherical reflectance (“white-sky albedo”) (42) and therefore is directly comparable with both modeled and spectrometer albedo values. Like the MOD09GA surface reflectance products, MOD10A1 was resampled (nearest neighbor) to a pixel size of 500 × 500 m, reprojected to North Pole Stereographic (ESRI:102018), and clipped to the GIMP ice mask. All pixels flagged as clouds in either the MOD10A1 or the coincident MOD09GA cloud-state layer were excluded from the analysis.

Daily downward shortwave radiation was obtained from MAR3.9 (26). A climatology of downward shortwave radiation was produced by averaging data over the 2001–2017 period resulting in 92 downward shortwave radiation fields (one for every day of the summer). Like the albedo data, the daily downward shortwave radiation data were reprojected to North Pole Stereographic, resampled (nearest neighbor) to 500 × 500 m pixels, and clipped to the GIMP ice mask (37).

### Gap filling

We interpolated almost all the missing values (i.e., pixels flagged as cloud) in the MODIS bare ice classification and albedo products from 2001 to 2017 using a gap-filling method. Missing pixels were reclassified on the basis of the value of the same pixel in the antecedent grid. If the same pixel in the antecedent grid was also missing, then the preceding grid was used to reclassify the pixel. This process was repeated incrementally up to 3 days before and after the original grid. The gap filling reduced the fraction of missing pixels from 59 to 0.7%.

### Ablation zone

The ablation zone, where the annual melt and runoff exceed the snow accumulation rate and the SMB is negative, was defined using daily SMB data from MAR3.9 (26). For each grid cell, we summed the SMB values over the 2001–2017 period and defined the ablation zone as an SMB of <0.

### Net shortwave radiation

Net shortwave radiation at each pixel was calculated by subtracting the pixel albedo from one and multiplying by the daily downward shortwave radiation at that pixel. We first partitioned the net shortwave radiation absorbed by bare ice and firn/snow in the ablation zone for every summer between 2001 and 2017 using observed, seasonally evolving albedo of each surface type. Next, we calculated the mean bare ice and firn/snow albedo observed on June 1 during the 2001–2017 study period. The albedo of bare ice and firn/snow was then fixed to these mean values (0.55 and 0.78, respectively), and we recalculated the net shortwave radiation received by bare ice and firn/snow. The residual difference between bare ice or firn/snow with observed albedo versus bare ice or firn/snow with fixed albedo allowed us to isolate the relative importance of the extent and albedo of bare ice and firn/snow on net shortwave radiation in the ablation zone.

To evaluate the sensitivity of our results to the choice of fixed bare ice albedo value, we repeated the net shortwave radiation analysis while incrementally increasing and decreasing the fixed bare ice albedo by  $\pm 0.01$  from the original value (0.55). We find that the bare ice–albedo feedback only becomes stronger than the snowline-albedo feedback when the fixed albedo of bare ice is raised by +0.12 (to 0.67). The conclusion of our study (that snowline migration is a primary amplifier of melt and that bare ice or firn/snow albedo are secondary in comparison) therefore appears robust to uncertainties in the choice of fixed bare ice albedo that, when averaged across the ablation zone, are not expected to be greater than  $\pm 0.02$ .

### RCM bare ice extent and snowline

Daily bare ice extent was derived from two RCMs commonly used for future projections of Greenland SMB: MAR3.9 (26) and RACMO2.3p2 (30). To discriminate between bare ice and snow pixels in RACMO2.3p2, we used an albedo threshold of <0.55. In MAR3.9, bare ice pixels were identified as those with a density between 915 and 925 kg m<sup>-3</sup> at a depth of 0 cm and an albedo of less than 0.60.

Both models were coupled to multilayer, one-dimensional snow models that explicitly simulate surface albedo as a function of snow grain size and impurity content. When snowpack thickness reaches zero, MAR3.9 prescribes an initial bare ice albedo of 0.55, which can decrease depending on the depth of water layer covering the ice to a minimum of 0.35 and increase depending on clouds and solar zenith angle to 0.60. RACMO2.3p2 calculates bare ice albedo as the 5% lowest surface albedo measured by the MODIS 16-day albedo product (MCD43A3) during the 2001–2010 period. The daily bare ice extent maps from the models were used to calculate a summer bare ice presence index in the same way as for the MODIS composite products. To enable comparison between different products, we resampled all products to a 1-km grid using bilinear interpolation. We then clipped all bare ice presence index maps to a common mask based on the GIMP ice mask and calculated the end-of-summer bare ice extent and snowline elevation for each model (fig. S2).

Note that some approaches for hindcasting Greenland melt and runoff directly incorporate observed albedo from MODIS. For example, the albedo field of HIRHAM5 (43) is based on de-noised MOD10A1 surface albedo. Both snow and bare ice were therefore observed (i.e. spatially and temporally variable), and HIRHAM5 implicitly captured the strength of the snowline-albedo and bare ice–albedo feedback. By incorporating observed albedo from MODIS, (43) shows that discrepancies between observed and modeled ice sheet melt and runoff are substantially reduced. However, this approach is not applicable for future projections of Greenland SMB, since observations of surface albedo are not available. Accurate predictions of Greenland’s future meltwater runoff contributions to global sea level are therefore likely to rely on refining snowpack models to more accurately determine the timing of bare ice exposure and associated strength of the snowline-albedo feedback.

### SUPPLEMENTARY MATERIALS

Supplementary material for this article is available at <http://advances.sciencemag.org/cgi/content/full/5/3/eaav3738/DC1>

Fig. S1. Sensitivity of each IMBIE sector to the snowline-albedo feedback during the 2001–2017 study period.

Fig. S2. Difference between observed (MODIS) bare ice presence index and that modeled by RACMO2.3p2 and MAR3.9 in an average melt year (2005) and high melt year (2016).



Fig. S3. Example of random forests classification of bare ice and snow in West Greenland on 25 July 2016.

Fig. S4. Feature space occupied by water, land, bare ice, and snow in MOD09GA visible and near-infrared bands.

Fig. S5. Frequency of bare ice exposure (i.e., presence index) during summer 2012 in Southwest Greenland (IMBIE sector 6).

Fig. S6. Mean number of valid MODIS pixel observations across the Greenland Ice Sheet for each summer month between 2001 and 2017.

Fig. S7. Relationship between MODIS bare ice presence index with that derived from 21 AWSs situated across the Greenland Ice Sheet between 2009 and 2017.

Table S1. Maximum (or end-of-summer) snowline and bare ice extent for IMBIE sectors 1 to 4 between 2001 and 2017.

Table S2. Maximum (or end-of-summer) snowline elevation and bare ice extent for IMBIE sectors 5 to 8 between 2001 and 2017.

## REFERENCES AND NOTES

1. X. Chen, X. Zhang, J. A. Church, C. S. Watson, M. A. King, D. Monselesan, B. Legresy, C. Harig, The increasing rate of global mean sea-level rise during 1993–2014. *Nat. Clim. Chang.* **7**, 492–495 (2017).
2. J. L. Chen, C. R. Wilson, B. D. Tapley, Satellite gravity measurements confirm accelerated melting of Greenland Ice Sheet. *Science* **313**, 1958–1960 (2006).
3. E. Rignot, I. Velicogna, M. R. van den Broeke, A. Monaghan, J. T. M. Lenaerts, Acceleration of the contribution of the Greenland and Antarctic ice sheets to sea level rise. *Geophys. Res. Lett.* **38**, L05503 (2011).
4. M. van den Broeke, J. Bamber, J. Ettema, E. Rignot, E. Schrama, W. J. van de Berg, E. van Meijgaard, I. Velicogna, B. Wouters, Partitioning recent Greenland mass loss. *Science* **326**, 984–986 (2009).
5. E. M. Enderlin, I. M. Howat, S. Jeong, M.-J. Noh, J. H. van Angelen, M. R. van den Broeke, An improved mass budget for the Greenland ice sheet. *Geophys. Res. Lett.* **41**, 866–872 (2014).
6. M. R. Van Den Broeke, E. M. Enderlin, I. M. Howat, P. K. Munneke, B. P. Y. Noël, W. J. Van De Berg, E. Van Meijgaard, B. Wouters, On the recent contribution of the Greenland ice sheet to sea level change. *Cryosphere* **10**, 1933–1946 (2016).
7. J. E. Box, X. Fettweis, J. C. Stroeve, D. K. Hall, K. Steffen, Greenland ice sheet albedo feedback: Thermodynamics and atmospheric drivers. *Cryosphere* **6**, 821–839 (2012).
8. C. R. Steger, C. H. Reijmer, M. R. van den Broeke, The modelled liquid water balance of the Greenland Ice Sheet. *Cryosphere* **11**, 2057–2526 (2017).
9. M. van den Broeke, J. Box, X. Fettweis, E. Hanna, B. Noël, M. Tedesco, D. van As, W. J. van de Berg, L. van Kampenhout, Greenland Ice Sheet surface mass loss: Recent developments in observation and modeling. *Curr. Clim. Change Rep.* **3**, 345–356 (2017).
10. M. Tedesco, X. Fettweis, M. R. van den Broeke, R. S. W. van de Wal, C. J. P. P. Smeets, W. J. van de Berg, M. C. Serreze, J. E. Box, The role of albedo and accumulation in the 2010 melting record in Greenland. *Environ. Res. Lett.* **6**, 014005 (2011).
11. M. Tedesco, S. Doherty, X. Fettweis, P. Alexander, J. Jeyaratnam, J. Stroeve, The darkening of the Greenland ice sheet: Trends, drivers, and projections (1981–2100). *Cryosphere* **10**, 477–496 (2016).
12. W. Greuell, Melt–water accumulation on the surface of the Greenland ice sheet: Effect on albedo and mass balance. *Geogr. Ann. Ser. A Phys. Geogr.* **82**, 489–498 (2016).
13. I. G. M. Wientjes, R. S. W. Van de Wal, G. J. Reichert, A. Sluijs, J. Oerlemans, Dust from the dark region in the western ablation zone of the Greenland ice sheet. *Cryosphere* **5**, 589–601 (2011).
14. M. Stibal, J. E. Box, K. A. Cameron, P. L. Langen, M. L. Yallop, R. H. Mottram, A. L. Khan, N. P. Molotch, N. A. M. Christmas, F. Cali Quaglia, D. Remias, C. J. P. P. Smeets, M. R. van den Broeke, J. C. Ryan, A. Hubbard, M. Tranter, D. van As, A. P. Ahlström, Algae drive enhanced darkening of bare ice on the Greenland Ice Sheet. *Geophys. Res. Lett.* **44**, 11463–11471 (2017).
15. A. J. Tedstone, J. L. Bamber, J. M. Cook, C. J. Williamson, X. Fettweis, A. J. Hodson, M. Tranter, Dark ice dynamics of the south-west Greenland Ice Sheet. *Cryosphere* **11**, 2491–2506 (2017).
16. C. J. Williamson, A. M. Anesio, J. Cook, A. Tedstone, E. Poniecka, A. Holland, D. Fagan, M. Tranter, M. L. Yallop, Ice algal bloom development on the surface of the Greenland Ice Sheet. *FEMS Microbiol. Ecol.* **94**, fiy025 (2018).
17. J. C. Ryan, A. Hubbard, M. Stibal, T. D. Irvine-Fynn, J. Cook, L. C. Smith, K. Cameron, J. Box, Dark zone of the Greenland Ice Sheet controlled by distributed biologically-active impurities. *Nat. Commun.* **9**, 1065 (2018).
18. L. C. Smith, R. R. Forster, B. L. Isacks, D. K. Hall, Seasonal climatic forcing of alpine glaciers revealed with orbital synthetic aperture radar. *J. Glaciol.* **43**, 480–488 (1997).
19. A. G. Klein, B. L. Isacks, Spectral mixture analysis of Landsat thematic mapper images applied to the detection of the transient snowline on tropical Andean glaciers. *Glob. Planet. Change* **22**, 139–154 (1999).
20. A. Rabatel, A. Bermejo, E. Loarte, A. Soruco, J. Gomez, G. Leonardini, C. Vincent, J. E. Sicart, Can the snowline be used as an indicator of the equilibrium line and mass balance for glaciers in the outer tropics? *J. Glaciol.* **58**, 1027–1036 (2012).
21. C. S. Benson, Stratigraphic studies in the snow and firn of the Greenland Ice Sheet (US Army Cold Reg. Res. Lab, Hanover, NH, 1962), CRREL Res. Rep. 70, pp. 24–26.
22. M. Fahnestock, R. Bindshadler, R. Kwok, K. Jezek, Greenland Ice Sheet surface properties and ice dynamics from ERS-1 SAR imagery. *Science* **262**, 1530–1534 (1993).
23. K. C. Partington, Discrimination of glacier facies using multi-temporal SAR data. *J. Glaciol.* **44**, 42–53 (1998).
24. M. R. van den Broeke, P. Smeets, J. Ettema, C. van der Veen, R. van de Wal, J. Oerlemans, Partitioning of melt energy and meltwater fluxes in the ablation zone of the west Greenland ice sheet. *Cryosphere* **2**, 179–189 (2008).
25. S. Hofer, A. J. Tedstone, X. Fettweis, J. L. Bamber, Decreasing cloud cover drives the recent mass loss on the Greenland Ice Sheet. *Sci. Adv.* **3**, e1700584 (2017).
26. X. Fettweis, J. E. Box, C. Agosta, C. Amory, C. Kittel, C. Lang, D. van As, H. Machguth, H. Gallée, Reconstructions of the 1900–2015 Greenland ice sheet surface mass balance using the regional climate MAR model. *Cryosphere* **11**, 1015–1033 (2017).
27. D. Van As, A. B. Mikkelsen, M. H. Nielsen, J. E. Box, L. C. Lijedahl, K. Lindbäck, L. Pitcher, B. Hasholt, Hypsometric amplification and routing moderation of Greenland ice sheet meltwater release. *Cryosphere* **11**, 1371–1386 (2017).
28. A. Mikkelsen, A. L. Hubbard, M. MacFerrin, J. E. Box, S. H. Doyle, A. Fitzpatrick, B. Hasholt, H. L. Bailey, K. Lindbäck, R. Pettersson, Extraordinary runoff from the Greenland Ice Sheet in 2012 amplified by hypsometry and depleted firn-retention. *Cryosph. Discuss.* **9**, 4625–4660 (2015).
29. M. Vizcaino, W. H. Lipscomb, W. J. Sacks, M. van den Broeke, Greenland surface mass balance as simulated by the community earth system model. Part II: Twenty-first-century changes. *J. Climate* **27**, 215–226 (2014).
30. B. Noël, W. J. van de Berg, J. M. van Wessem, E. van Meijgaard, D. van As, J. T. M. Lenaerts, S. Lhermitte, P. Kuipers Munneke, C. J. P. P. Smeets, L. H. van Ulf, R. S. W. van de Wal, M. R. van den Broeke, Modelling the climate and surface mass balance of polar ice sheets using RACMO2—Part 1: Greenland (1958–2016). *Cryosphere* **12**, 811–831 (2018).
31. B. Noël, W. J. van de Berg, E. van Meijgaard, P. K. Munneke, R. S. W. van de Wal, M. R. van den Broeke, Evaluation of the updated regional climate model RACMO2. 3: Summer snowfall impact on the Greenland Ice Sheet. *Cryosphere* **9**, 1831–1844 (2015).
32. B. Franco, X. Fettweis, M. Erpicum, Future projections of the Greenland ice sheet energy balance driving the surface melt. *Cryosphere* **7**, 1–18 (2013).
33. M. Mengel, A. Levermann, K. Frieler, A. Robinson, B. Marzeion, R. Winkelmann, Future sea level rise constrained by observations and long-term commitment. *Proc. Natl. Acad. Sci. U.S.A.* **113**, 2597–2602 (2016).
34. M. Mengel, A. Nauels, J. Rogelj, C.-F. Schleussner, Committed sea-level rise under the Paris Agreement and the legacy of delayed mitigation action. *Nat. Comms.* **9**, 601 (2018).
35. K. A. Casey, C. M. Polashenski, J. Chen, M. Tedesco, Impact of MODIS sensor calibration updates on Greenland Ice Sheet surface reflectance and albedo trends. *Cryosphere* **11**, 1781–1795 (2017).
36. J. C. Ryan, A. Hubbard, T. D. Irvine-Fynn, S. H. Doyle, J. M. Cook, M. Stibal, J. E. Box, How robust are in situ observations for validating satellite-derived albedo over the dark zone of the Greenland Ice Sheet? *Geophys. Res. Lett.* **44**, 6218–6225 (2017).
37. I. M. Howat, A. Negrete, B. E. Smith, The Greenland Ice Mapping Project (GIMP) land classification and surface elevation data sets. *Cryosphere* **8**, 1509–1518 (2014).
38. L. Breiman, Random forests. *Mach. Learn.* **45**, 5–32 (2001).
39. A. P. Ahlström, D. van As, M. Citterio, S. B. Andersen, R. S. Fausto, M. L. Andersen, R. Forsberg, L. Stenseng, E. L. Christensen, S. S. Kristensen, A new programme for monitoring the mass loss of the Greenland ice sheet. *Geol. Surv. Denmark Greenl. Bull.* **15**, 61–64 (2008).
40. D. van As, A. L. Hubbard, B. Hasholt, A. B. Mikkelsen, M. R. van den Broeke, R. S. Fausto, Large surface meltwater discharge from the Kangerlussuaq sector of the Greenland ice sheet during the record-warm year 2010 explained by detailed energy balance observations. *Cryosphere* **6**, 199–209 (2012).
41. J. M. Shea, B. Menounos, R. D. Moore, C. Tennant, An approach to derive regional snow lines and glacier mass change from MODIS imagery, western North America. *Cryosphere* **7**, 667–680 (2013).
42. J. C. Stroeve, J. E. Box, T. Haran, Evaluation of the MODIS (MOD10A1) daily snow albedo product over the Greenland ice sheet. *Remote Sens. Environ.* **105**, 155–171 (2006).
43. P. L. Langen, R. S. Fausto, B. Vandecrux, R. H. Mottram, J. E. Box, Liquid water flow and retention on the Greenland Ice Sheet in the regional climate model HIRHAM5: Local and large-scale impacts. *Front. Earth Sci.* **4**, 110 (2017).

**Acknowledgments:** We thank Polar Field Services Inc. and Kangerlussuaq International Science Support (KISS) for providing the logistical support that assisted the conceptualization of the manuscript, with assistance from K. Young, S. Zager, and K. Cosper. We also thank

H. Johnson (Brown University) for computing support. RCM outputs from MAR3.9 were provided by X. Fettweis. RCM outputs from RACMO2.3p2 were provided by B. Noël and M. van den Broeke. **Funding:** This research was funded by a NASA Cryosphere Program grant managed by T. P. Wagner. **Author contributions:** J.C.R. conceptualized the project, developed the methodology, carried out the data analysis, and wrote the original manuscript. L.C.S. acquired the funding, provided supervision, assisted with development of the methodology, and co-wrote the manuscript. D.v.A., S.W.C., M.G.C., L.H.P., and A.H. assisted with development of the methodology and edited the manuscript. **Competing interests:** The authors declare that they have no competing interests. **Data and materials availability:** All data needed to evaluate the conclusions in the paper are present in the paper and/or the Supplementary Materials. Additional data related to this paper may be requested from the authors. All data can also be accessed online from the following data centers: MOD09GA and Landsat data from <https://lpdaac.usgs.gov>, maintained by the NASA EOSDIS LP DAAC at the USGS/EROS Center,

Sioux Falls, South Dakota; MOD10A1 data from <https://nsidc.org/data/mod10a1>, maintained by the National Snow and Ice Data Center DAAC at Boulder, Colorado; and AWS data from GAP/PROMICE (<https://promice.org/DataDownload.html>).

Submitted 20 September 2018

Accepted 27 January 2019

Published 6 March 2019

10.1126/sciadv.aav3738

**Citation:** J. C. Ryan, L. C. Smith, D. van As, S. W. Cooley, M. G. Cooper, L. H. Pitcher, A. Hubbard, Greenland Ice Sheet surface melt amplified by snowline migration and bare ice exposure. *Sci. Adv.* **5**, eaav3738 (2019).

## Greenland Ice Sheet surface melt amplified by snowline migration and bare ice exposure

J. C. Ryan, L. C. Smith, D. van As, S. W. Cooley, M. G. Cooper, L. H Pitcher and A. Hubbard

*Sci Adv* 5 (3), eaav3738.

DOI: 10.1126/sciadv.aav3738

### ARTICLE TOOLS

<http://advances.sciencemag.org/content/5/3/eaav3738>

### SUPPLEMENTARY MATERIALS

<http://advances.sciencemag.org/content/suppl/2019/03/04/5.3.eaav3738.DC1>

### REFERENCES

This article cites 42 articles, 5 of which you can access for free  
<http://advances.sciencemag.org/content/5/3/eaav3738#BIBL>

### PERMISSIONS

<http://www.sciencemag.org/help/reprints-and-permissions>

Use of this article is subject to the [Terms of Service](#)